RASĀYAN *J. Chem.*
Vol. 19 | No. 4 | 2019-2029 | October-December | 2026
ISSN: 0974-1496 | e-ISSN: 0976-0083 | CODEN: RJCABP
http://www.rasayanjournal.com
http://www.rasayanjournal.co.in

FABRICATION OF ZINC OXIDE NANOPARTICLES USING ABELMOSCHUS ESCULENTUS: GREEN SYNTHESIS, CHARACTERIZATION, AND CYTOTOXICITY STUDIES AGAINST MCF-7 CELL LINES

R. Surve[1,✉], S. Bhagawati[2], M. Kopparam[2], Pradeep H. K.[3], R. Sawant[1], and N. Shivathaya[1]

[1]Department of Pharmaceutics, Rani Chennamma College of Pharmacy, Belagavi-590010, Karnataka, India
[2]Department of Pharmaceutics, Sree Siddaganga College of Pharmacy, Tumkur-572013, Karnataka, India
[3]Department of Pharmaceutics, GM Institute of Pharmaceutical Sciences and Research, Davanagere-577006, Karnataka, India
✉Corresponding author: rashmisurve8514@gmail.com

ABSTRACT

The solution combustion process was effectively employed to develop zinc oxide nanoparticles by using aqueous extract of *Abelmoschus esculentus* (okra) as a natural stabilising and reducing agent, providing an economical and environmentally responsible substitute for traditional chemical synthesis. Formation of nanoparticles was indicated by yellowish colouration of the reaction mixture and verified with UV spectroscopy, showing a distinctive absorption peak at ~360 nm. XRD analysis verified the hexagonal wurtzite crystalline structure of ZnO, while FTIR spectroscopy identified –OH, N–H & C=O functional groups, evidencing the role of okra phytochemicals in nanoparticle capping and stabilisation. SEM revealed aggregated, porous particles (93–234 nm), whereas TEM confirmed non-spherical, polycrystalline particles of 20–40 nm. DLS analysis showed a hydrodynamic size of approximately 150 nm with a zeta potential of 0.5 mV, indicating moderate colloidal stability. The MTT assay demonstrated a concentration-dependent reduction in the viability of Michigan Cancer Foundation-7 (MCF-7) breast cancer cells, indicating promising anticancer potential. The porous morphology significantly enhances surface reactivity, rendering the synthesised ZnO-NPs highly suitable for biomedical, antimicrobial, and photocatalytic applications. The study contributes to the field of green nanotechnology by introducing a sustainable method for producing bioactive ZnO nanoparticles and presents a basis for future studies on the development of nanomedicines for cancer. The results align with Sustainable Development Goal-3:Good Health and Well-being through sustainable technologies to support health care.

Keywords: Zinc Oxide, Okra, Nanoparticles, Green Synthesis.

RASĀYAN *J. Chem.*, Vol. 19, No.4, 2026

INTRODUCTION

Nanotechnology is a focal point of research in contemporary materials science. This technology can offer various novel applications, including advanced fabric materials, food processing, agricultural production, and intricate medical treatments.[1] It encompasses the synthesis, characterisation, and exploration of materials within the nanometre scale. This technology involves materials whose structures demonstrate significantly improved physicochemical and biological properties, along with unique phenomena and functionalities due to their nanoscale dimensions.[2] The nanoscale dimensions often provide nanoparticles (NPs) with greater surface areas than macro-sized particles.[3] Due to their diminutive dimensions, nanoparticles possess a greater surface area-to-volume ratio. This unique characteristic enables potential applications in various domains, including nanomedicine, bionanotechnology, and biosensors.[3] The inherent characteristics of metal nanoparticles, including silver, titanium dioxide (TiO_2), and zinc oxide (ZnO), are primarily defined by their crystallinity, composition, shape, and size. Minimising dimensions to the nanoscale can alter their optical, mechanical, structural, morphological, chemical, and electrical

http://doi.org/10.31788/RJC.2026.1949925

characteristics. These altered characteristics enable the nanoparticles to engage distinctively with cellular biomolecules, hence promoting the physical translocation of nanoparticles into the intracellular structures.[4] Nanostructured materials possess a higher proportion of surface atoms, resulting in increased surface reactivity. Consequently, nanomaterials have recently gained considerable significance in both fundamental and practical sciences, as well as in bionanotechnology. Various researchers have investigated the various morphologies of nanosized ZnO and revealed that it has significant antibacterial properties against a extensive range of bacterial species.[5-11] "ZnO" is presently under examination as an antibacterial agent in both nanoscale and microscale formulations. ZnO demonstrates considerable antibacterial properties when its particle size is diminished to the nanometre scale, allowing nano-sized ZnO to engage with bacterial surfaces and/or penetrate the bacterial core, thereby revealing unique bactericidal pathways. The particular compounds have been utilised for the antibacterial applications, especially in the food industry, although their interactions with bacteria are primarily damaging. Several studies reveal that ZnO-NPs are compatible with human cells[12], as a result it can be employed as antibacterial agents that are detrimental to micro-organisms and have good compatibility with human cells. Nanoparticles exhibit unique physicochemical properties and high effective surface area compared to volume ratios, which are primarily responsible for their diverse antibacterial potential. Nevertheless, the exact mechanisms remain contentious, despite the suggestion and adoption of various theories. Research on antibacterial nanomaterials, primarily ZnO nanoparticles, will advance the field of nanomaterials and elucidate the mechanisms and phenomena associated with nanostructured materials. A major health issue, it has attracted notice from people all around the world as a threat to human health; bacterial transmissible illnesses have social and economic repercussions. Significant worldwide health risks to humans, especially children, include rising outbreaks & infections of bacterial antibiotic resistance, the introduction of novel bacterial mutations, pathogenic strains, the lack of suitable immunisations in developing countries, and hospital-acquired illnesses. Every year, Shigella flexneri infections cause 1.5 million deaths due to the bacteria's contamination of food and drink.[13] Therefore, it is crucial to create novel antibacterial medications that target bacterial strains, especially significant foodborne pathogens such as Salmonella, Staphylococcus aureus, Campylobacter jejuni, Pseudomonas aeruginosa, Enterococcus faecalis, and *E. coli.* This investigation focuses on the objective of a green synthesis approach to develop Zinc oxide nanoparticles, specifically the precipitation method, with okra aqueous extract as the reducing agent. There is limited information on the synthesis of ZnO nanoparticles using *Abelmoschus esculentus* (okra) aqueous extract through the solution precipitation method and their subsequent evaluation against MCF-7 breast cancer cells. The effects of Zn $(NO_3)_2$ concentration and temperature on the particle size of the synthesised nanoparticles were evaluated. UV-visible spectroscopy, SEM, FTIR, XRD, and TEM studies were used to characterise the produced ZnO-NPs. Okra fruit aqueous extract was selected for this study due to its abundant content of bioactive chemicals, such as polysaccharides, phenolic acids, flavonoids, and mucilage, which are known as natural stabilising and reducing agents. These compounds facilitate the eco-friendly and cost-effective synthesis of nanoparticles by eliminating the need for harmful chemical reagents.

Additionally, the extract's availability, biocompatibility, and ease of preparation further justify its use in green synthesis methods, aligning with the principles of sustainable and environmentally friendly nanotechnology. In sustainable development and fabrication of Zinc-Oxide nanoparticles (ZnO NPs), the interaction between chemical precursors and plant-derived phytochemicals is the fundamental mechanism that determines the size, shape, and stability of the resulting particles. The precursor is the chemical salt that provides the zinc ions (Zn^{2+}) necessary for the formation of the nanoparticle's crystal lattice. In phytogenic synthesis, these precursors must be water-soluble to interact effectively with the aqueous plant extracts.

This work can contribute to the United Nations Sustainable Development Goal (SDG-3): Good Health and Well-being by developing the eco-friendly zinc oxide nanoparticles with biomedical applications against breast cancer. This work introduces a sustainable green synthesis strategy using extract from the Abelmoschus esculentus (okra) and highlights the potential for developing eco-friendly and safe therapeutic interventions. The results will help drive sustainable healthcare technologies and research on nanomedicine.

EXPERIMENTAL

Materials

Fresh okra (Abelmoschus esculentus) pods were procured from the local market in Belagavi, Karnataka, India. Botanical authentication was carried out by Dr. Harsha V. Hegde, and a voucher specimen was deposited in the herbarium with accession number RMRC-1752. The zinc nitrate hexahydrate ($Zn(NO_3)_2 \cdot 6H_2O$, ≤99%) salt was sourced as the precursor for the preparation of zinc oxide nanoparticles. All other chemicals used in the study were of laboratory grade and procured from SD Fine, Loba Chem Pvt. Ltd.

Preparation of Aqueous Extract of Okra Fruits

The collected okra pods were thoroughly cleaned with purified water to get rid of adhering impurities and dirt. Cleaned pods were shade-dried at room temperature for 72 h, followed by drying at 30–40°C until a constant weight was achieved. The dried material was pulverised using an electric blender, passed through sieve #22, and stored in an airtight container for further use. For preparation of the aqueous extract, 20 g of powder was added to 100 mL of purified water in a boiling flask. The mixture was heated to its boiling point for 2 h to ensure the complete extraction of bioactive components. The extract was allowed to cool to room temperature after boiling. To get a clean filtrate, the cooled extract was taken for filtration using Whatman filter paper or a fine muslin cloth. The filtrate was then subjected to evaporation on a water bath to reduce its volume to half of the original quantity. The concentrated filtrate was collected, transferred to a clean, airtight container and refrigerated at 4°C for further use.[14]

Synthesis of Zinc Oxide Nanoparticles

A series of zinc nitrate hexahydrate [$Zn(NO_3)_2 \cdot 6H_2O$] solutions of varying molar concentrations were prepared in 50 mL of purified water. Followed by, 20 mL of aqueous extract was added dropwise while being stirred magnetically at 70 °C for about 4 h, and the pH was adjusted as specified in Table-1. Centrifugation was used to collect the precipitate, followed by calcination in a muffle furnace at 450°C for a period of 3 h to obtain ZnO nanoparticles.

Table-1: Fabrication of ZnO Nanoparticles

Trials	Molarity of Zinc Nitrate	pH	Responses Particle size (nm)
1	0.01	6	155
2	0.05	6	175
3	0.01	10	135
4	0.05	10	165
5	0.0017	8	151
6	0.058	8	181
7	0.03	5.2	165
8	0.03	10.8	155
9	0.03	8	139
10	0.03	8	140
11	0.03	8	142

Characterization

UV–visible Spectroscopy

The optical characteristics and structural conformation of ZnO nanoparticles were investigated using Ultraviolet-Visible (UV-Vis) spectroscopy, performed on a Shimadzu UV-1900I spectrophotometer at ambient temperature. To find distinctive absorption bands linked to the production of nanoparticles, spectral measurements were performed over a wavelength range of 200-800 nm.

Fourier Transform Infrared (FTIR) analysis

ZnO-NPs functional groups were identified using the FTIR Spectroscopic method. The analysis was performed using a Bruker FTIR spectrophotometer at Poornayu Research Lab, Bangalore, Karnataka, India. Spectra were captured over a wavenumber range of 500– 4000 cm^{-1}, and the potassium bromide (KBr) pellet technique was utilised for sample preparation prior to measurement.[15]

X-ray Diffraction

The crystallinity index of the ZnO-NPs samples was evaluated to assess the degree of crystalline ordering within the desired size range. Powder X-ray diffraction (P-X R D) patterns were captured using a "Rigaku MiniFlex" 300/600 diffractometer. Prior to analysis, the nanosuspensions were converted into dry powder form through a solvent exchange method, employing acetone as the exchanging solvent to facilitate complete removal of water without disrupting the crystalline structure.[15]

Surface Morphology and Elemental Composition (SEM–EDX)

A SEM (S-3400, Hitachi, Japan) fitted with an energy dispersive X-Ray (EDX) detector was used to analyse the surface topology and elemental composition of developed ZnO- NPs. To reduce the charging effects, dried nanoparticle powder was placed on carbon tape that was fastened to an aluminium stub and sputter–coated with a thin layer of gold. Captured the SEM images at magnifications ranging from ×3000 to ×6000 using an accelerating voltage of 10 kV and a working distance of 6.7 mm. Particle size estimation was performed by measuring multiple particles directly from the SEM micrographs using the instrument's image analysis software.

Transmission Electron Microscopy (TEM)

The morphological characteristics of the optimised ZnO-NPs were examined through "Transmission Electron Microscopy" (TEM) analysis. An FEI Tecnai G2 transmission electron microscope with a Field Emission Gun (FEG) Source and a intensifying voltage of 200 kV was employed to capture the images, and a computer-controlled liquid nitrogen (LiN_2) cryostage capable of tilting up to ±80 degrees.

Particle Size Distribution and Zeta Potential

The hydrodynamic particle size dispersion of the biosynthesised ZnO-NPs was determined using a Microtrac FLEX Particle Size Analyser (Version 11.0.0.2). The nanoparticles were dispersed in distilled water (refractive index 1.33; viscosity 0.833 cP at 27.97°C) prior to analysis. A set-zero calibration was performed for 30s, followed by a single 90s measurement under standard sensitivity and normal resolution conditions. During measurement, the reflected laser power was maintained at 0.74 µW, and the cell temperature was approximately 28°C. Zeta potential measurements were carried out using the Microtrac Zetatrac module coupled with the FLEX system to evaluate the charges on the surface and dispersible stability in aqueous medium of ZnO-NPs. Measurements were performed at 27.97 °C with a dispersant pH of 7, viscosity of 0.833 cP, and dielectric constant of 79. Electrophoretic mobility was recorded under an applied electric field strength of 1.4 kV/m.

MTT Assay / Toxicity Studies

Trypsinised monolayer cell culture was used; the cell count of 5.0×10^5 cells/ml was adjusted using the 10% FBS. 100 µL of the diluted suspension having 5.0 x 10^4 cells/well was added to an individual well of a 96-microtiter plate. The supernatant layer was removed after 24 h, then washed with the medium. The various concentrations of test drug in 100 µL were incorporated into each well. The incubation period was set for 37°C in a 5% CO_2 atmosphere for 24 h. On completion of the incubation period, the test solutions were discarded, followed by the addition of 100µL of MTT solution of concentration 5.0 mg/ 10 mL of MTT solution in PBS to each well. Incubating the plates for 4h at 37° C containing 5% of Carbon dioxide in atmosphere. Following incubation, the supernatant was discarded, and 100 µL of DMSO was added. These plates were shaken gently to dissolve the formazan crystals. A microplate reader was employed to capture absorbance at 590 nm. Each cell line dose-dependent response curve was used to calculate the IC50 values. The below-mentioned formula was employed to determine the percentage of growth inhibition:

$$\% \text{ of Inhibition} = \frac{\text{OD of Control - OD of Sample}}{\text{OD of Control}} \text{ X } 100$$

RESULTS AND DISCUSSION

UV–visible Spectroscopy

The reaction mixture exhibited a yellow colour, which indicates that ZnO-NPs had formed. The variation of colours in the reaction mixture confirmed the green synthesis. The Okra extract in distilled water added

to Zn^{+2} solution exhibited the dark grey colour to yellow at the adjusted pH mentioned in the Table-1. The green-synthesised ZnO-NPs were analysed using a UV–Vis spectrophotometer over the optical absorption range. A characteristic absorption peak was observed at ~360 nm, confirming the formation of ZnO-NPs.-1: UV Spectrum of Zinc Oxide Nanoparticles.

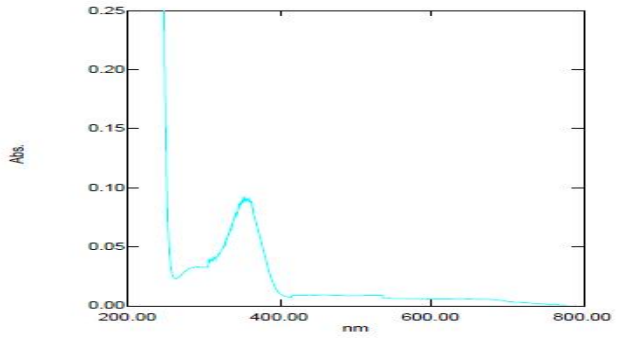

Fig.-1: UV Spectrum of Zinc Oxide nanoparticles

Fourier Transform Infrared (FTIR) Analysis

The structural characteristics of the synthesised ZnO-NPs were analysed using FTIR spectroscopy, indicating the involvement of phytomolecules from the plant extract in stabilising the reaction intermediates. The broad peak in ~3296 cm^{-1} correlates with –OH stretching vibrations of alcohols/phenolic groups, while the band at 2915 cm^{-1} is attributed to aliphatic C–H stretching, indicating the existence of lipid or oil components. The peak observed at 2847 cm^{-1} is assigned to stretching of N-H vibrations of secondary amines. The presence of carbonyl groups is represented by the absorption band at 1730 cm^{-1}, which is attributable to C=O stretch vibrations. The sharp peak at 1607 cm^{-1} corresponds to N–H bending vibrations, suggesting the presence of primary and secondary amides and amines. The band observed at ~1422 cm^{-1} is assigned to $–CH_3$ bending vibrations of alkanes. Additionally, the broad absorption in the range of 950–1110 cm^{-1} may be attributed to C–O, C–N, or C–X (halide) stretching vibrations, as illustrated in Fig.-2.

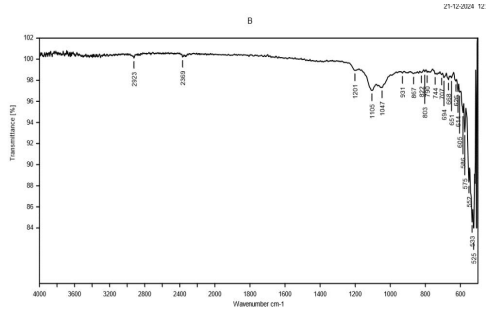

Fig.-2: FTIR of Green Synthesised Zinc Oxide Nanoparticles

X-ray Diffraction (XRD)

The XRD pattern of the synthesized ZnO-NPs (Fig. 4) shows well-defined 2θ values having diffraction peaks like 31.69°, 34.37°, 36.18°, 47.48°, 56.50°, 62.81°, 66.27°, 67.87°, 68.99°, 72.53°, and 76.91°, which are indexed to the (110), (002), (101), (100), (103), (102), (104), (202), (112), (201), and (200) planes, respectively as shown in Fig.-3. The diffraction pattern is consistent with the characteristic wurtzite hexagonal structure of ZnO, as reported in the literature.

Surface Morphology and Elemental Composition (SEM-EDX)

The SEM micrographs (Fig.-4), reveal that the synthesized ZnO material exhibits nanoscale features. The smaller particles (~93.5 nm and ~99.2 nm) represent the nanoscale dimensions of ZnO, while the larger structures (~198 nm and ~234 nm) likely correspond to agglomerates formed due to the intrinsic tendency of nanoparticles to cluster. The surface appears rough and porous, which is a characteristic feature of ZnO nanoparticles, enhancing their surface area and reactivity.

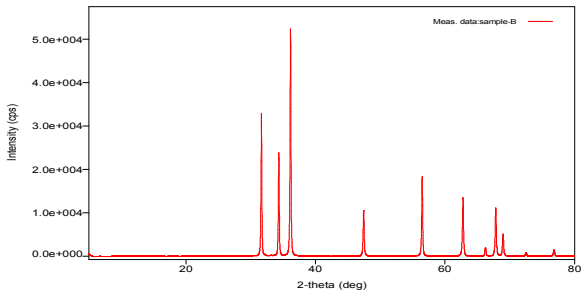

Fig.-3: X-ray Diffraction Pattern of *Abelmoschus esculentus* ZnO NPs

The severe clustering creates a dense, three-dimensional porous network defined by the spacing between the large agglomerates. This high degree of macro-porosity (inter-particle volume) is a critical, beneficial structural feature for applications that rely on bulk gas diffusion or fluid infiltration, such as gas sensing, catalysis, antimicrobial treatments or filtration, where access to a large interconnected volume is necessary. The uniform distribution of particles, coupled with visible agglomeration, may influence the material's performance, depending on the intended application. EDX analysis (Table-2) confirmed the successful formation of zinc oxide, with Zn (71.80 wt%) and O (24.37 wt%) appearing as the dominant elements. Trace amounts of C, K, and Ca were also detected, which may correspond to phytochemical residues from the plant extract used during green synthesis. The high zinc content and the Zn:O atomic ratio obtained from the spectrum suggest good purity and effective conversion of the zinc precursor into ZnO nanoparticles. Collectively, the SEM and EDX results (Fig.-5) demonstrated that the synthesised nanoparticles were nanosized, slightly aggregated, and compositionally consistent with ZnO produced via green synthesis.[13]

Table-2: Quantitative Results of EDX Analysis of ZnO NPs

Element Line	Weight%	Weight% Error	Atom %
C K	1.84	± 1.07	5.42
O K	24.37	± 0.98	53.93
K K	0.85	± 0.22	0.77
Ca K	1.14	± 0.22	1.00
Zn K	71.80	± 3.71	38.88
Total	100.00		100.00

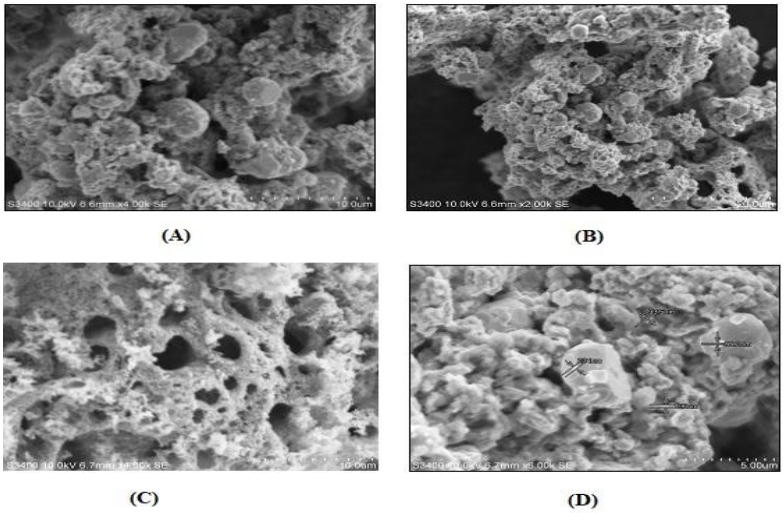

Fig.-4: SEM images (a-d) of ZnONPs using Abelmoschus Esculentus Fruit Extract

Transmission Electron Microscopy (TEM)

TEM micrographs (Fig.-6) demonstrated that zinc oxide nanoparticles are erratic, slightly aggregated clusters composed of smaller crystalline domains. At higher magnification, the particles appeared

nanoscale with semi-distinct boundaries, indicating that individual primary particles had fused to form larger agglomerates.

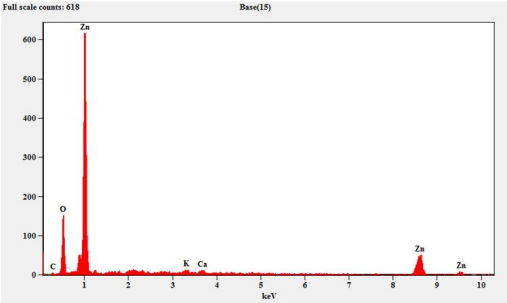

Fig.-5: EDX Spectra of ZnO Nanoparticles

The particle size observed in the finer regions was typically below 20–30 nm, while the aggregated masses extended to around 150–250 nm. The internal lattice fringes visible in the high-resolution images validated that the produced Zn-O nanoparticles were crystalline. The SAED pattern displayed well-defined concentric diffraction rings, indicating a polycrystalline structure. These rings correlate to characteristic planes of hexagonal wurtzite ZnO, ensuring successful development of crystalline zinc oxide. The combination of TEM imaging and SAED analysis verifies that the green-synthesised ZnO nanoparticles possess nanoscale crystalline domains embedded within aggregated structures, consistent with plant-mediated nanoparticle formation.

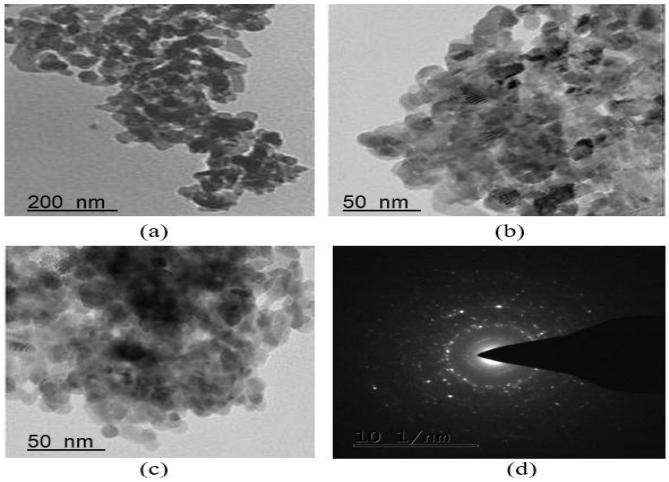

Fig.-6: (a), (b), (c) TEM Image of Synthesized ZnO NPs (d) SAED Pattern

Particle Size Distribution and Zeta Potential

The particle size dispersion of ZnO-NPs fabricated via the precipitation method and aqueous extract of Okra was determined by dynamic light scattering (DLS). The size dispersion, as depicted in the graph, primarily falls between 50 nm and 300 nm, with a notable peak around 100 nm. This suggests that most of the nanoparticles are concentrated within this size range, indicating a relatively narrow size distribution. The red histogram, which represents the % passing through different size ranges, shows that about 90% of the nanoparticles are below 200 nm, reflecting the synthesis method's efficiency in producing nanoparticles with uniform sizes.

The green curve on the graph, representing the intensity distribution, indicates the number of particles in each size channel. The steep rise in the curve around 50 nm to 100 nm further supports that the majority of particles are within this size range. The low zeta potential value (0.5 mV) indicates that the nanoparticles have a weak electrostatic repulsion, which may suggest that they are more prone to agglomeration in suspension. A higher zeta potential typically correlates with better stability, as particles with stronger repulsion forces are less likely to aggregate.

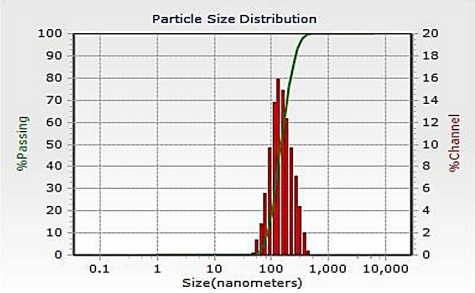

Fig.-7: Average Particle Size Distribution of ZnO-NPs

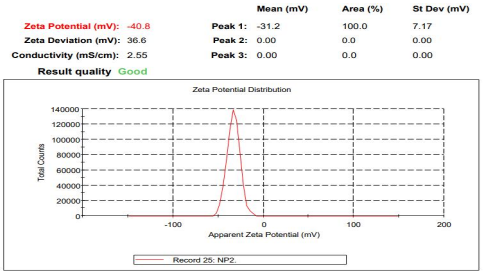

Fig.-8: Zeta Potential of Synthesised Abelmoschus esculentus ZnONPs

MTT Assay / Toxicity studies

The cytotoxic activity of doxorubicin (positive control), green-synthesised zinc oxide nanoparticles, and the aqueous fruit extract of *Abelmoschus esculentus* was evaluated against the MCF-7 human breast cancer cell line using the MTT assay. The assay measures mitochondrial metabolic activity through the enzymatic reduction of MTT to insoluble purple formazan crystals by viable cells, thereby serving as an indicator of cell viability. The percentage of viable cells decreased in a concentration-dependent manner following treatment with all test samples (Table-3 and Fig.-9).

Doxorubicin (Sample I) exhibited the highest cytotoxic activity throughout the tested concentration range. Cell viability remained below 11% even at the lowest concentration (10 µg/mL) and further decreased to 3.8 ± 1.0% at 320 µg/mL, corresponding to approximately 89.7–96.2% growth inhibition. The strong cytotoxic response observed for doxorubicin confirms its established efficacy as a potent chemotherapeutic agent and validates the sensitivity of the MTT assay. The green-synthesised zinc oxide nanoparticles (Sample II) demonstrated significantly greater cytotoxicity than the crude aqueous extract. Cell viability decreased progressively from 41.2 ± 2.1% at 10 µg/mL to 10.4 ± 1.7% at 320 µg/mL, while growth inhibition increased from 58.8% to 89.6%, indicating a pronounced dose-dependent antiproliferative effect.

The enhanced cytotoxic activity of the nanoparticles may be attributed to their nanoscale dimensions, high surface area, improved cellular internalisation, and efficient interaction with intracellular targets. Previous studies have demonstrated that ZnO nanoparticles induce excessive intracellular reactive oxygen species (ROS) generation, mitochondrial membrane depolarisation, oxidative DNA damage, and activation of apoptotic signalling pathways, ultimately resulting in cancer cell death. In comparison, the aqueous fruit extract of *A. esculentus* (Sample III) exhibited moderate cytotoxic activity. Cell viability gradually declined from 91.2 ± 2.3% at 10 µg/mL to 45.2 ± 1.9% at 320 µg/mL, corresponding to 8.8–54.8% growth inhibition.

Although the extract displayed a clear concentration-dependent inhibitory effect on MCF-7 cell proliferation, its cytotoxic potential was considerably lower than that of the synthesised nanoparticles. This activity is likely associated with the presence of naturally occurring phytoconstituents, including flavonoids, phenolic compounds, and quercetin, which have been reported to suppress cancer cell proliferation by inducing apoptosis, regulating the cell cycle, and modulating oxidative stress. The markedly enhanced cytotoxicity of the ZnO nanoparticles compared with the crude extract suggests that nanoparticle synthesis substantially improves the biological activity of the phytoconstituents present in *A. esculentus.*

Table-3: Cytotoxicity of Doxorubicin, ZnO Nanoparticles and Aqueous Extract Against MCF-7 Cells Determined by MTT Assay

S. No.	Concentration (µg/mL)	Sample I (Doxorubicin) Cell Viability (%)	Sample II (ZnO Nanoparticles) Cell Viability (%)	Sample III (Aqueous Extract) Cell Viability (%)
1	10	10.3 ± 1.2	41.2 ± 2.1	91.2 ± 2.3
2	20	9.7 ± 1.5	38.6 ± 2.6	89.8 ± 2.8
3	40	6.1 ± 1.3	32.9 ± 2.3	80.5 ± 2.2
4	80	7.4 ± 1.6	23.4 ± 1.8	53.6 ± 2.1
5	160	4.2 ± 1.1	15.6 ± 2.2	48.7 ± 2.0
6	320	3.8 ± 1.0	10.4 ± 1.7	45.2 ± 1.9

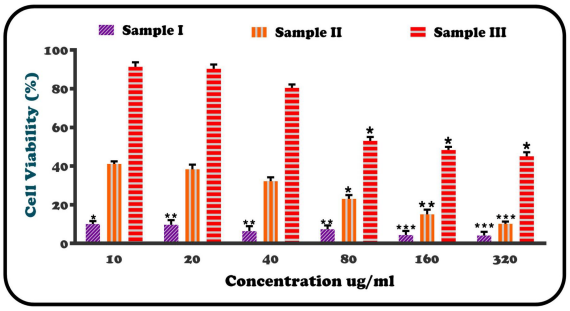

Fig.-9: Cytotoxicity of Doxorubicin, ZnO Nanoparticles and Aqueous Extract Against MCF-7 Cells Determined by MTT Assay

Comparative Analysis of Phytogenic ZnO NP Synthesis with their Application

Table-4: Comparative Summary of Green-Synthesized ZnO Nanoparticles from different Plant Sources and their Applications, Including Abelmoschus Esculentus in the Present Anticancer Study on MCF-7 Cells

Plant Source	Zinc Precursor	UV-Vis Peak	Primary Application	Article Reference
Hibiscus rosa-sinensis (Leaves)	Zinc nitrate hexahydrate	295-340 nm	Photocatalytic dye degradation (81.3%) & Antimicrobial	[16]
Artocarpus altilis (Leaf/Stem Bark)	Zinc sulphate	290–340 nm	Antioxidant, Anti-inflammatory & Antibacterial	[17]
Brassica oleracea (Cabbage)	Fresh Extract	380 nm	Antibacterial (*E. coli*, *S. pyogenes*)	[18]
Syzygium aromaticum (Clove)	Zinc nitrate	366 nm	Dental restorative (GIC) & *S. mutans* inhibition	[19]
Punica granatum (Pomegranate peel)	Plant extract fuel	374 nm	Antibacterial against *S. pyogenes*	[20]
Abelmoschus esculentus (Okra)	Zinc nitrate hexahydrate	~360 nm	Biomedical & Anticancer Activity on MCF-7 Breast Cells	Current Study

Table-5: Comparative Analysis of Method of Preparation with Others

Feature	Okra (Current study)/ pomegranate	Hibiscus / Clove / Artocarpus [19, 20]
Synthesis Speed	Very rapid (minutes once combustion starts)	Slower (2–4 hours of stirring)
Role of Extract	Fuel + Reducer + Stabilizer	Reducer + Stabilizer
Agglomeration	Higher (due to rapid gas evolution)	Lower (more control over particle growth)
Washing Steps	Minimal	Multiple centrifugation/washing cycles required

Comparison of plant sources influences the diversity (as shown in Table-5); the plant source directly impacts the nanoparticle properties. While leaf extracts like *Hibiscus* typically produce smaller particles (~26 nm), the use of fruit/mucilage-based extracts like Okra provides a robust natural "scaffold" for

growth. This results in the highly stable, porous structures observed in our SEM analysis, which achieve significant efficiency in environmental remediation and biomedical applications compared to denser particles from sources like pomegranate.

CONCLUSION

The present study successfully demonstrated a cost-effective and eco-friendly "green" synthesis of Zinc Oxide (ZnO) nanoparticles using the aqueous fruit extract of *Abelmoschus esculentus* (Okra). Phytochemicals found in the extract serve as effective reducing and stabilizing agents, eliminating the need for toxic chemicals. Characterisation via UV-Vis spectroscopy confirmed the formation of nanoparticles with a characteristic peak at 360 nm, while XRD and SAED patterns verified the high crystallinity and hexagonal wurtzite structure of the product. FTIR analysis confirmed the presence of bioactive functional groups responsible for the synthesis of nanoparticles. SEM and TEM analysis showed a spherical shape with a size within the nanoparticle range. The high zinc content (71.80 wt%) and porous morphology suggest that these nanoparticles are well-suited for biomedical applications. Furthermore, the synthesised ZnO nanoparticles, taken for cytotoxicity studies using the MTT assay on MCF-7 cell lines, demonstrated a concentration-dependent decline in cell viability, confirming their anticancer potential. Although the activity was comparatively lower than the standard drug, the nanoparticles showed significant biological effects at higher concentrations. These findings collectively suggest that the green-synthesised ZnO nanoparticles possess promising anticancer properties, making them suitable candidates for further development in pharmaceutical and biomedical applications.

ACKNOWLEDGMENTS

The authors sincerely acknowledge Poornayu Research Lab, Bangalore, Karnataka, and Infinite Biotech, Institute of Research and Analytics, Sangli, Maharashtra, for their timely support, valuable assistance, and prompt delivery of results throughout the course of this research work. Their cooperation and efficient analytical services significantly contributed to the successful completion of the study.

CONFLICT OF INTERESTS

The authors declare that there is no conflict of interest.

AUTHOR CONTRIBUTIONS

The present work is related to *SDG-3: Good Health and Well-being*. All the authors contributed significantly to this manuscript, participated in reviewing/editing and approved the final draft for publication. The research profile of the authors can be verified from their ORCID ids, given below:

Rashmi Surve https://orcid.org/0000-0003-0334-9702
Siddalingappa Bhagawati https://orcid.org/0009-0008-9770-8123
Manjunath Kopparam https://orcid.org/0000-0003-2301-4539
Pradeep H. K. https://orcid.org/0000-0003-2416-132X
Reshma Sawant https://orcid.org/0009-0000-7026-9409
Neha Shivathaya https://orcid.org/0000-0002-8188-0075

Cite this article as: R. Surve *et al.*, *Rasayan J. Chem.*, 19(4), 2019-2029(2026), https://doi.org/10.31788/RJC.2026.1949925

REFERENCES

1. S. Sahoo, 2010 *10th IEEE Conference Nanotechnology* NANO, 1205(2010), https://doi.org/10.1109/NANO.2010.5697887
2. S. Pal, Y.K Tak, J.M Song, *Applied and Environmental Microbiology,* **73**, 1712(2007), https://doi.org/10.1128/AEM.02218-06
3. N. Joudeh, D. Linke. Journal of Nanobiotechnology, **262(20)**, 1(2022), https://doi.org/10.1186/s12951-022-01477-8

4. J. W Rasmussen, E. Martinez, P. Louka, D. G Wingett, *Expert Opinion on Drug Delivery,* **7**, 1063(2010), https://doi.org/10.1517/17425247.2010.502560
5. K.R Raghupathi, R.T Koodali, A.C Manna, *Langmuir,* **27**, 4020(2011), https://doi.org/10.1021/LA104825U
6. Padmavathy N, Vijayaraghavan R, *Science and Technology of Advanced Materials*, **9**, 035004(2008), https://doi.org/10.1088/1468-6996/9/3/035004
7. E.K Zarrindokht, *African Journal of Microbiology Research*, **5(12)**, 1369(2011), https://doi.org/10.5897/AJMR10.159
8. J. T Seil, T. J Webster, *International Journal of Nanomedicine,* **7**, 2767(2012), https://doi.org/10.2147/IJN.S24805
9. R. Jalal, E. K Goharshadi, M. Abareshi, M. Moosavi, A. Yousefi, P. Nancarrow, *Materials Chemistry and Physics,* **121**, 198(2010), https://doi.org/10.1016/J
10. N. Jones, B. Ray, K. T Ranjit, A. C Manna, *FEMS Microbiology Letters*, **279**, 71(2008). https://doi.org/10.1111/J.1574-6968.2007.01012.X
11. R. Brayner, R. Ferrari Iliou, N. Brivois, S. Djediat, M.F Benedetti, F. Fievet, *Nano Letters,* **6**, 866(2006), https://doi.org/10.1021/NL052326H
12. G. Colon, B.C Ward, T.J Webster, *Journal of Biomedical Materials Research A,* **78**, 595(2006). https://doi.org/10.1002/JBM.A.30789
13. https://pubmed.ncbi.nlm.nih.gov/10516787
14. S. Selim, S.S Salem, M.E Owda, M.S Almuhayawi, H.S Gattan, M.H Alruhaili, *Green Process Synthesis,***14**, 1(2025), https://doi.org/10.1515/gps-2024-0218
15. P.H Keshavamurthysetty, D.H Patel, *Indian Journal of Pharmaceutical Education and Research,* **57(s)**, 32(2023), https://doi.org/10.5530/ijper.57.1s.5
16. S.A Rabi, A.J.S Kennedy, *Asian Journal of Chemistry.* **37**(8), 2037(2025), https://doi.org/10.14233/AJCHEM.2025.34076
17. B. Prathibha, S. Nair, V. Gnana, G. Kanmoni, *Asian Journal of Chemistry,* **38(4)**, 963(2026), https://doi.org/10.14233/AJCHEM.2026.35495
18. S. Rajeshkumar, H. Agarwal, S. Venkat Kumar, T. Lakshmi, *Asian Journal of Chemistry,* **30(12)**,2711(2018), https://doi.org/10.14233/AJCHEM.2018.21562
19. N. Ahalya, P. Dhamodhar, A.D Vaishnavi, *Asian Journal of Chemistry,* **33(3)**, 515(2021), https://doi.org/10.14233/AJCHEM.2021.23037
20. S. Akash, N. Ahalya, P. Dhamodhar, *Asian Journal of Chemistry,* **32(4)**, 907(2020), https://doi.org/10.14233/AJCHEM.2020.22495

[RJC-9925/2026]